Journal of Alloys and Compounds 501 (2010) 60–66

Contents lists available at ScienceDirect

Journal of Alloys and Compounds

journal homepage: www.elsevier.com/locate/jallcom

3C-SiC nanowires and micro-scaled polyhedra: Synthesis, characterization and properties

Qiaolian Pang[a,b], Liqiang Xu[a,b,*], Zhicheng Ju[a,b], Zheng Xing[a,b], Lishan Yang[a,b], Qin Hao[a,b], Yitai Qian[a,b,*]

[a] Key Laboratory of Colloid and Interface Chemistry (Shandong University), Ministry of Education, Jinan, Shandong, 250100, PR China
[b] School of Chemistry and Chemical Engineering, Shandong University, Jinan 250100, PR China

ARTICLE INFO

Article history:
Received 6 February 2010
Received in revised form 30 March 2010
Accepted 1 April 2010
Available online 10 April 2010

Keywords:
Silicon carbide
Nanostructured materials
Transmission electron microscopy
X-ray diffraction
Scanning electron microscopy

ABSTRACT

Cubic phase silicon carbide (3C-SiC) nanowires (labeled as "Sample 1") with diameters ranging from 10 nm to 80 nm and lengths up to several micrometers were obtained by using CHI_3, Si powder, and metallic Na as reactants at 230 °C. In addition, SiC polyhedra (labeled as "Sample 2") with smooth surfaces and diameters of 2–5 μm were obtained by using the different amounts of the same reactants at 500 °C. The room-temperature photoluminescence (PL) spectra of Sample 1 and Sample 2 show strong ultraviolet emission peaks centered at 360 nm and 354 nm, respectively. Thermal gravimetric analysis (TGA) curves reveal that the thermal stability (against air oxidation) of Sample 2 is better than Sample 1. The possible formation mechanisms of the products with distinct dimensions were briefly discussed.

1. Introduction

The synthesis of silicon carbide (SiC) materials has aroused great research interests because of their diverse superior properties, which make it useful in functional ceramic and high temperature semiconductor fields [1–4]. SiC has large number of polytypes such as 3C-SiC, 4H-SiC, 6H-SiC etc.; moreover, 3C-SiC shows the highest electron mobility [5,6]. Therefore, 3C-SiC has a potential application in high power and high frequency devices [7]. In the literature, many indications show that the properties (e.g. optical properties) of SiC display strong dependences on their morphologies and sizes [8–14]. Compared with SiC nanostructures [9–20], there were few reports on the SiC micro-scaled polyhedra [21–23]. The investigation on the synthesis and properties of micro-scaled polyhedra will not only enrich the morphology science of SiC but also provide new enlightenment for the synthesis of large-sized SiC single crystals, which may broaden the potential applications of SiC semiconductor materials in the future [24].

Conventionally, the methods for the preparation of 3C-SiC nanocrystals always need high temperature, for instance, carbothermal reduction, self-propagating, sol–gel, and so on [25–29]. In this case, synthesis of SiC at low temperature is still a practical challenge. Most recently, 3C-SiC had been synthesized at low temperature, for example, a sulfur-assisted reduction route ($Si–S–Na–C_2Cl_4$) at 130 °C [30], using Na–K alloy as reductants ($SiCl_4–Na–K–CHBr_3$) at 130 °C [9], and by the system of $SiO_2–C_2H_5OH–Mg$ at 200 °C [31].

Herein, we report a simple but effective method for the fabrication of 3C-SiC nanowires by using metallic Na, Si powder and CHI_3 in a stainless-steel autoclave at 230 °C; While SiC micro-scaled polyhedra with high yields also could be produced by using about twice amounts of the same reactants at 500 °C. The reaction temperature and the amounts of carbon source were found to be crucial for the formation of the SiC with different morphologies.

2. Experimental

2.1. Preparation of samples

All the reagents (Shanghai Chemical Reagents Company) used in these experiments were of analytical grade and were used without further purification. [Warning: Metal Na and K are chemical active reductants, for security, the experimental procedure should be done carefully and quickly.]

Sample 1 was prepared as follows: Na (1.527 g), Si powders (0.500 g), and CHI_3 (7.017 g) were mixed in a 22-ml stainless-steel autoclave. After tightly sealed, the autoclave was maintained at 230 °C for 20 hours (h) and then cooled to room temperature naturally. The raw products in the autoclave were collected and washed with absolute alcohol, dilute HCl, hot concentrated 70% $HClO_4$ (at 180 °C for 3 h), and the mixture of $HF–HNO_3$ (v/v = 1:3), respectively, in order to remove the alkali metal halides, amorphous carbon and Si. Finally, the gray product was washed with

* Corresponding authors at: School of Chemistry and Chemical Engineering, Shandong University, Shanda Nanlu 27, Jinan, Shandong 250100, China.
Tel.: +86 531 8836 6280; fax: +86 531 8836 6280.
E-mail address: xulq@sdu.edu.cn (L. Xu).

0925-8388/$ – see front matter © 2010 Elsevier B.V. All rights reserved.
doi:10.1016/j.jallcom.2010.04.028

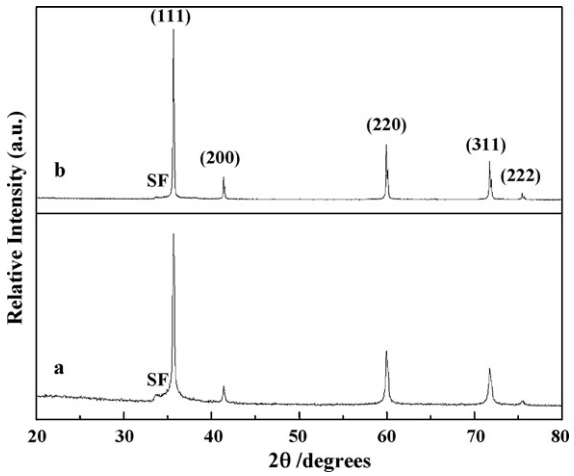

Fig. 1. XRD patterns of the final samples: (a) Sample 1; (b) Sample 2.

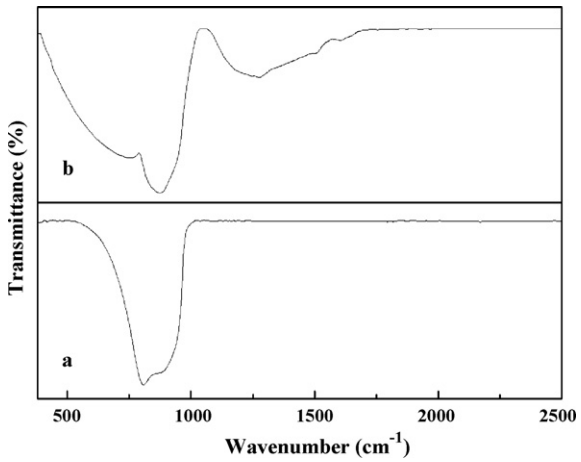

Fig. 2. FTIR spectra of the final samples: (a) Sample 1; (b) Sample 2.

distilled water and absolute alcohol for several times and then it was dried in a vacuum at 100 °C for 1 h.

Through tuning the amounts of the reactants (see Table 1: sign 8), the other sample was prepared. In order to remove the byproducts, the raw product was post-treated similarly with that of Sample 1. Then the solution containing the SiC product was stirred vigorously for several minutes and kept still for 5 min. The dispersion and sedimentation process were repeated several times. After drying in vacuum at 100 °C for 1 h, a sample with green color (labeled as Sample 2) was eventually obtained.

2.2. Sample characterization

The X-ray powder diffraction (XRD) were carried out on a Bruker D8 advanced X-ray diffractometer equipped with Ni-filtered Cu Kα radiation (λ = 1.5418 Å). Fourier transform infrared spectroscopy (FTIR) measurements were performed by a Bruker Alpha-T. The Raman spectra were obtained from a NEXUS 670 FT-IR Raman spectrometer. The morphology and structure of the products were investigated by transmission electron microscopy (TEM, Hitachi H-7000), high-resolution transmission electron microscopy (HRTEM, JEOL-2100, 200 kV), and field emission scanning electron microscopy (FESEM, JEOL JSM-6700F). Photoluminescence (PL) spectrum measurements were performed in an Edinburgh FLS 920 fluorescence spectrophotometer with a Xe lamp at room temperature. Thermal gravimetric analysis (TGA) was recorded on a SDT Q600 V8.0 Build 95 thermal analyzer apparatus under air flow.

3. Results and discussion

3.1. XRD, FTIR, and Raman analysis

Fig. 1a and b shows the typical XRD patterns of Sample 1 and Sample 2, respectively. The sharp peaks with strong diffraction intensity in the two patterns can be appropriately indexed to cubic SiC. The lattice parameters of the 3C-SiC cell calculated from these two patterns are 4.359 Å and 4.357 Å, which are consistent with the standard values for 3C-SiC (a = 4.358 Å, JCPDS card no. 65-0360). The low-intensity peaks marked with SF in Fig. 1a and b can be ascribed to the stacking faults in the crystals [32]. No noticeable diffraction peaks of other impurities such as Si, SiO_2, and C were detected in these patterns.

Fig. 2a and b shows the typical FTIR spectra of Sample 1 and Sample 2, respectively. The intense absorption peak positioned at 808 cm^{-1} in Fig. 2a (or 875 cm^{-1} in Fig. 2b) can be indexed to the transverse optical (TO) photons vibration mode of the Si–C bond, which is consistent with the earlier reports [9,33]. The weaker absorption peak centered at about 1275 cm^{-1} in Fig. 2b can also be assigned to the vibration mode of Si–C bond [34,35]. No obvious peaks of other impurities were detected in these two spectra.

Typical Raman spectra of Sample 1 and Sample 2 are shown in Fig. 3. It is clearly seen that the presence of two sharp peaks positioned at 792 cm^{-1} and 968 cm^{-1} in Fig. 3a (Sample 1), which are associated with the TO and LO phonons at the Γ point of β-SiC, respectively [30]. The Raman spectrum of the as-synthesized micro-scaled polyhedra (Sample 2) is shown in Fig. 3b, two sharp peaks centered at about 793 cm^{-1} and 969 cm^{-1} are also obviously observed. The intensity of the TO (Γ) phonon line is stronger than that of the LO (Γ) phonon line; The relative shift (3–8 cm^{-1}) of the peaks in the spectra compared to the bulk SiC may be attributed to the confinement effect and the stacking faults of the products [36,37]. The sharp peaks confirm that the as-synthesized two samples are well crystalline [38–40]. At the same time, the results are consistent with those of the above X-ray patterns.

3.2. PL and thermal analysis

Fig. 4 shows the room-temperature photoluminescence (PL) spectra (with the excitation wavelength of 220 nm) of the final

Table 1
Experimental results of the final products produced at different reaction conditions.

Sign	Na (g)	Si (g)	CHI_3 (g)	T (°C)	t (h)	Phase	Nanowires	Polyhedra
1	1.527	0.500	7.017	170	20	No SiC		
2	1.527	0.500	7.017	180	20	3C-SiC	50%	Low
3	1.527	0.500	7.017	230	20	3C-SiC	80%	Low
4	1.527	0.500	7.017	500	20	3C-SiC	50%	Low
5	2.997	1.000	7.011	500	20	3C-SiC	50%	Low
6	2.997	1.000	10.302	500	20	3C-SiC	40%	30%
7	2.997	1.000	12.002	500	20	3C-SiC	15%	50%
8	2.997	1.000	14.030	500	20	3C-SiC	5%	70%
9	2.997	1.000	14.030	230	20	3C-SiC	50%	Low
10	2.997	1.000	14.030	500	5	3C-SiC	Low	70%
11	2.997	1.000	14.030	500	10	3C-SiC	Low	70%
12	2.997	1.000	14.030	500	15	3C-SiC	Low	70%

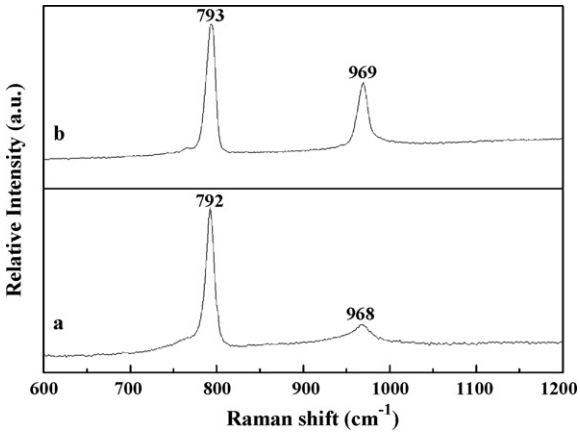

Fig. 3. Raman spectra of the final samples: (a) Sample 1; (b) Sample 2.

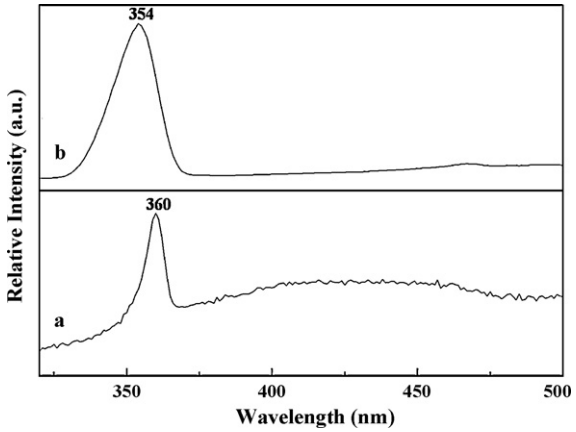

Fig. 4. Room-temperature PL spectra of the final samples: (a) Sample 1; (b) Sample 2.

SiC samples. Curve (a) and curve (b) show the PL spectra of Sample 1 and Sample 2, it can be clearly observed that peaks with strong intensity centered at 360 nm and 354 nm, respectively. Compared with the blue-green luminescence from the 3C-SiC films [41], the present emission peaks of the as-synthesized SiC products are indicative of blue-shift. This phenomenon might originate from the morphology, defects and quantum size effects [9,42], however, the exact luminescence mechanism still requires further interpretation.

In order to study the thermal stabilities (against air oxidation) of the samples, TGA was carried out under a flow of air in the temperature range of 40–1200 °C (see Fig. 5a). Initially, it is observed from TGA curves that both of them have a small peak in the temperature range of 40–360 °C. This may be attributed to the baseline drift of the TGA instrument (see Fig. 5b). Getting rid of the error from the instrument, curve a (I) shows almost no drastic weight gain or loss below 800 °C, while a gradual tiny weight gain suggests that SiC nanowires are oxidized in air atmosphere at temperatures above 800 °C. This result is in agreement with the previous reports [32,33]. When the temperature is raised above 1000 °C, curve a (I) correspondingly displays a drastic weight gain, indicating that the SiC nanowires sample is accelerated oxidized. Compared to curve a (I), curve a (II) is much smoother which does not show obvious weight gain or loss below 1200 °C. This may be ascribed to larger crystal size accordingly with smaller surface areas which result in their outstanding oxidation resistance [14,43]. These results show that the as-obtained sample especially the polyhedral products has good thermal stability (against air oxidation).

3.3. Morphology and growth mechanism of Sample 1

Detailed structure and morphology analysis of the products were further carried out with TEM and HRTEM. As shown in Fig. 6a, Sample 1 is mainly composed of one-dimensional SiC nanowires with uniform diameters about 60 nm and lengths up to several micrometers. The statistical TEM observation results indicate that the proportion of the nanowires (most of them have diameters about 60 nm, and a small part of them have diameters ranging from 10 nm to 80 nm) in the product is approximately 80%. It is found that almost one third of the obtained nanowires are bent. The quantum interference effect of the bent structure endowed the nanowires with new functions [44], for instance, it might provide potential application in nano-mechanics and nano-electron devices [45]. Fig. 6b shows the high-magnification TEM image of part of a randomly selected nanowire (in the lower-left corner), in which the interfringe distance of 0.25 nm is consistent with (1 1 1) interplanar distance of 3C-SiC, and the stacking faults could be observed. The corresponding fast Fourier transform (FFT) pattern (in the upper-right corner of Fig. 6b) indicates a streaking diffraction pattern characteristic of stacking faults. Combining this result with that of the XRD pattern (Fig. 1a), the appearance of low-intensity peak (marked with SF) is due to stacking faults of 3C-SiC. In addition, the [1 1 1] direction is parallel to the axis of the nanowire, implying that the nanowire might grow along the [1 1 1] direction.

In order to investigate the possible growth mechanism of the as-synthesized SiC nanowires, the raw product of Sample 1 (without treated with any solvents) was studied by TEM. As shown in Fig. 6c and d, it is found that solid particles exist at the tip or bending site of a SiC nanowire. This phenomenon is frequently found under TEM observations in our experiment. Solid particles located at the tip or bending site of these nanowires revealing that the as-obtained SiC nanowires may grow via a vapor–liquid–solid (VLS) growth mechanism [31,46,47]. Fig. 6e shows the XRD pattern of the raw product of Sample 1 without treated with any solvents, in which NaI, Si, and C are observed besides the cubic SiC. Fig. 6f shows a typical EDS spectrum of the raw product (without post treatment), indicating the raw product is mainly composed of SiC and NaI (based on the results of XRD pattern in Fig. 6e).

According to the aforementioned experimental results, the overall reaction involved in this experiment may be tentatively described as follows:

$$2CHI_3(g) + 6Na(l) + 2Si(s) \rightarrow 2SiC(s) + 6NaI(s) + H_2(g) \quad (1)$$

The reaction (1) may include the following reactions:

$$CHI_3(g) + 6Na(l) \rightarrow 6NaI(s) + H_2(g) + 2C(s) \quad (2)$$

$$Si(s) + C(s) \rightarrow SiC(s) \quad (3)$$

3.4. Morphology and growth mechanism of Sample 2

Fig. 7a shows the FESEM image of Sample 2. It can be seen that Sample 2 is mainly composed of polyhedron-like structures with sizes of 2–5 μm. Some typical images of individual polyhedra are shown in Fig. 7b1–b4, their multiple faces and smooth surfaces can be clearly seen, and the morphology of polyhedron in Fig. 7b1 is frequently observed in Sample 2. As the lattice fringes of micro-scaled polyhedra could hardly be clearly seen by HRTEM, we studied the small-scaled structure of Sample 2. Fig. 7c shows the HRTEM image of one typical layer (from Sample 2) with small scale. The clearly resolved interplanar spacing is about 0.25 nm, which corresponds to the (1 1 1) spacing of 3C-SiC. Fig. 7d shows the HRTEM image of a small particle (from Sample 2) near the edge (marked with S) of a polyhedron (in the lower-left corner of Fig. 7d), in which the interfringe distance of 0.25 nm is consistent with (1 1 1) interplanar

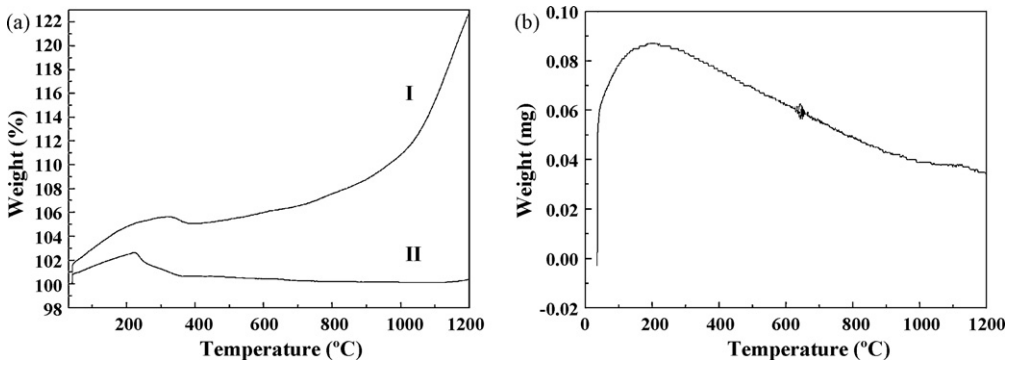

Fig. 5. (a) TGA analysis of the SiC samples, carried out under a stream of air, at heating rate of 10 °C/min: (I) Sample 1; (II) Sample 2. (b) TGA curve of the blank test.

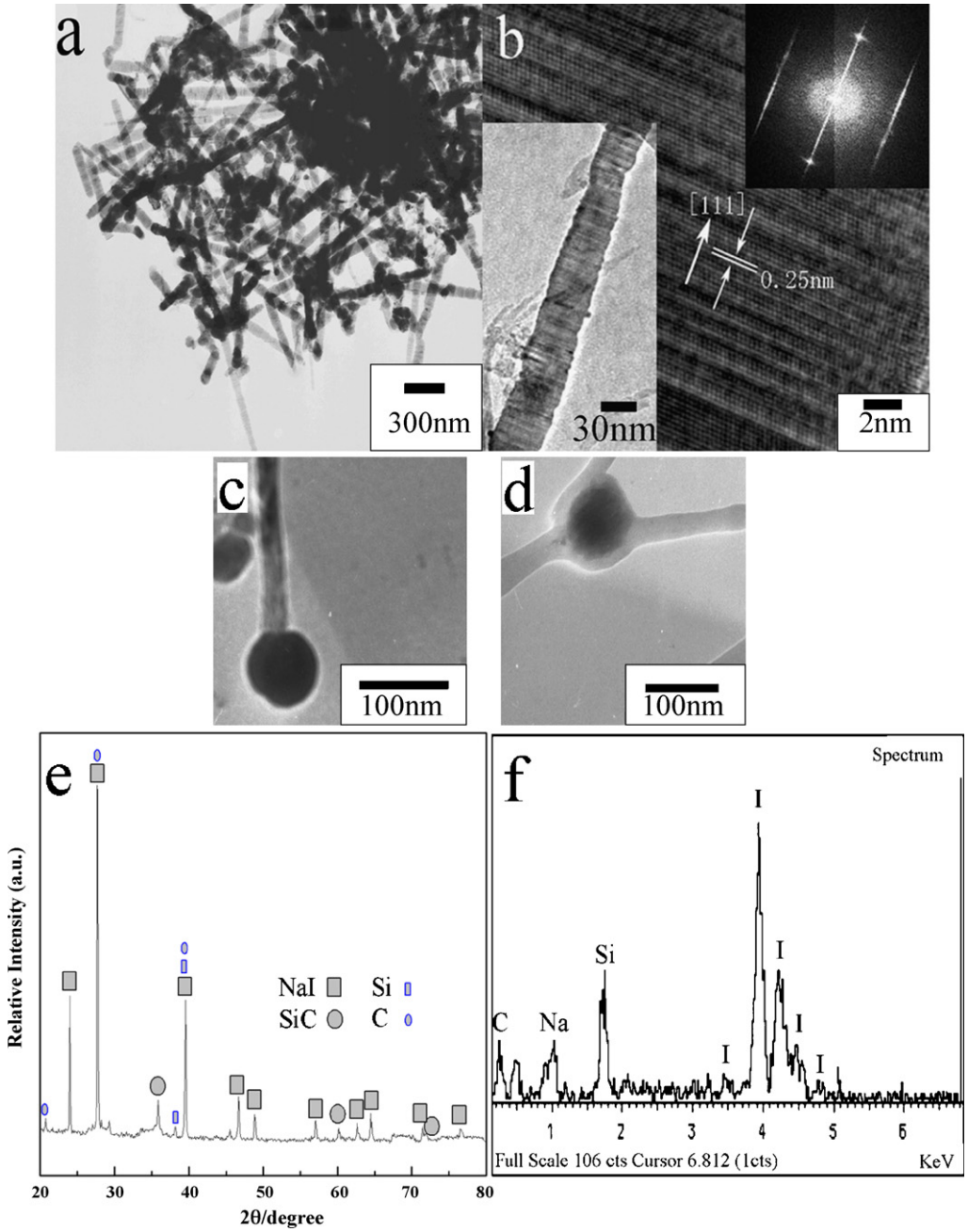

Fig. 6. (a) A typical TEM image of Sample 1. (b) HRTEM image of a part of a single nanowire. The inset shows its corresponding FFT pattern (upper) and TEM image of the nanowire (bottom). (c) TEM image of an individual nanowire attached with a solid particle. (d) TEM image of a curved nanowire attached with a solid particle. (e) XRD pattern of the raw product of Sample 1 without treated with any solvents. (f) A Typical EDS spectrum taken from the raw product without post treatment.

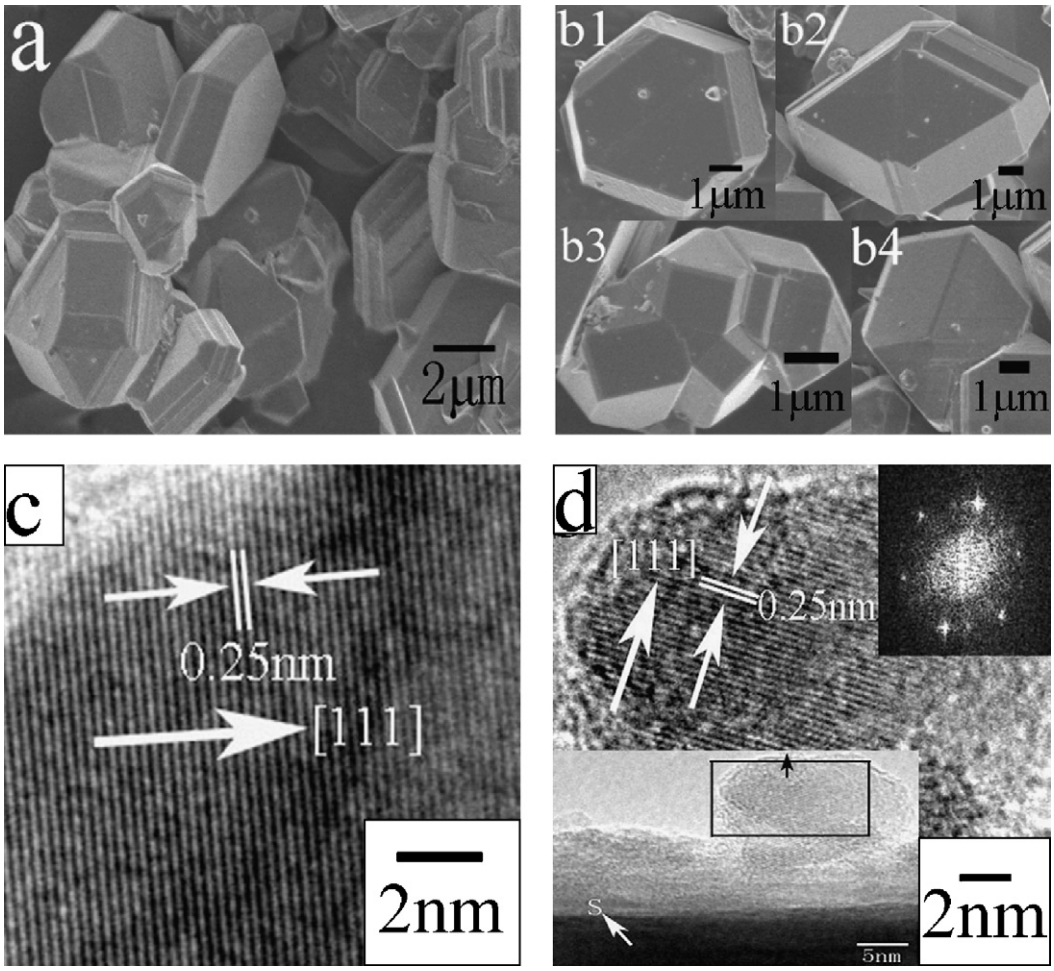

Fig. 7. (a) A typical FESEM image of Sample 2. (b1–b4) High-magnification FESEM images of some individual polyhedra. (c) HRTEM image of Sample 2 obtained from a typical layer which has small scale. (d) HRTEM image of a small particle near one edge of a polyhedron (marked with S in the bottom). The inset shows its corresponding FFT pattern (upper) and the low magnification TEM of the particle marked with a black square (bottom).

distance of 3C-SiC. The corresponding FFT pattern (in the upper-right corner of Fig. 7d) indicates that the twin crystal phenomena might exist in Sample 2.

The possible growth mechanism of the polyhedron is brief discussed as follows. As shown in Fig. 8, the formation of SiC micro-scaled polyhedra may undergo such a process. First, the SiC crystal experienced a two dimensional nucleation and formed a complete crystal layer (Fig. 8a), then the layer continued to grow based on layer-by-layer growth mode [48,49] and formed multilayered polyhedron-like structure (Fig. 8b), finally the multilayered polyhedron-like structure grown into polyhedron (Fig. 8c) under certain conditions. In general, the rate of the step generation is lower than that of the step movement, because the growth unit has to overcome the energy barrier caused by the increase in surface energy during the step generation. Thus, the layered steps disappeared while the perfect polyhedron formed. Conversely, if the rate of the step generation was higher than the step movement, the multilayered polyhedron-like structure would generate [50]. However, much work is still needed to explore the exact formation mechanism of 3C-SiC nanowires and micro-scaled polyhedra.

3.5. Influence of reaction conditions

To understand the effects of the reaction conditions on the formation of the SiC nanowires and micro-scaled polyhedra in the autoclave, a series of experiments (Table 1) have been conducted by varying the reaction temperatures or carbon sources. In our study, the autoclave is used as the reaction vessel which provides a sealed environment, and CHI_3 is used as the carbon source in the mean time to sustain a high pressure.

To investigate the effects of temperature, the reactions were carried out at different temperatures while keeping other parameters constant. When the temperature was set below 170 °C, almost no solid powders even amorphous or poorly crystalline SiC (obtained at 180 °C) could be collected (as shown in Table 1, signs 1 and 2). If the temperature was higher than 230 °C (e.g. 500 °C), the yield of SiC nanowires decreased (Table 1, sign 4). The results indicate that the relatively lower temperature is favourable for the formation of SiC nanowires.

Besides the reaction temperature, the amount of carbon source also has a significant effect on the yield of the SiC nanowires. The increase of the amount of CHI_3 could result in the lower ratio of SiC nanowires but high yield of SiC micro-scaled polyhedra (Table 1, signs 5–8). The yield of SiC nanowires would increase when the reaction temperature was decreased (Table 1, signs 8 and 9). Moreover, when the reaction time was shorten to 15 h, 10 h, 5 h, while the other parameters were kept constant with Sample 2, the morphology of the SiC micro-scaled polyhedra almost remained unchanged (Table 1, signs 10–12). But the yields of the final products were reduced.

Furthermore, different metals and carbon sources were also studied to explore the optimal routes for the synthesis of SiC micro-scaled polyhedra or nanowires (see Fig. 9). When K was used instead of Na, the reaction could occur at 140 °C; the XRD pat-

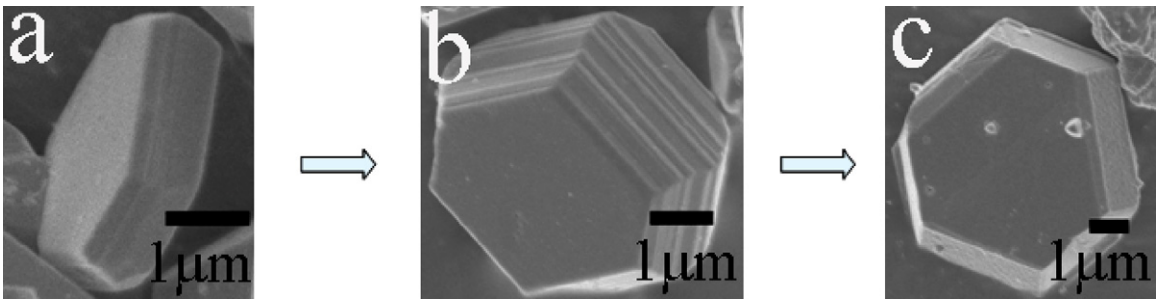

Fig. 8. FESEM images of Sample 2, which may demonstrate the growth mechanism of polyhedron.

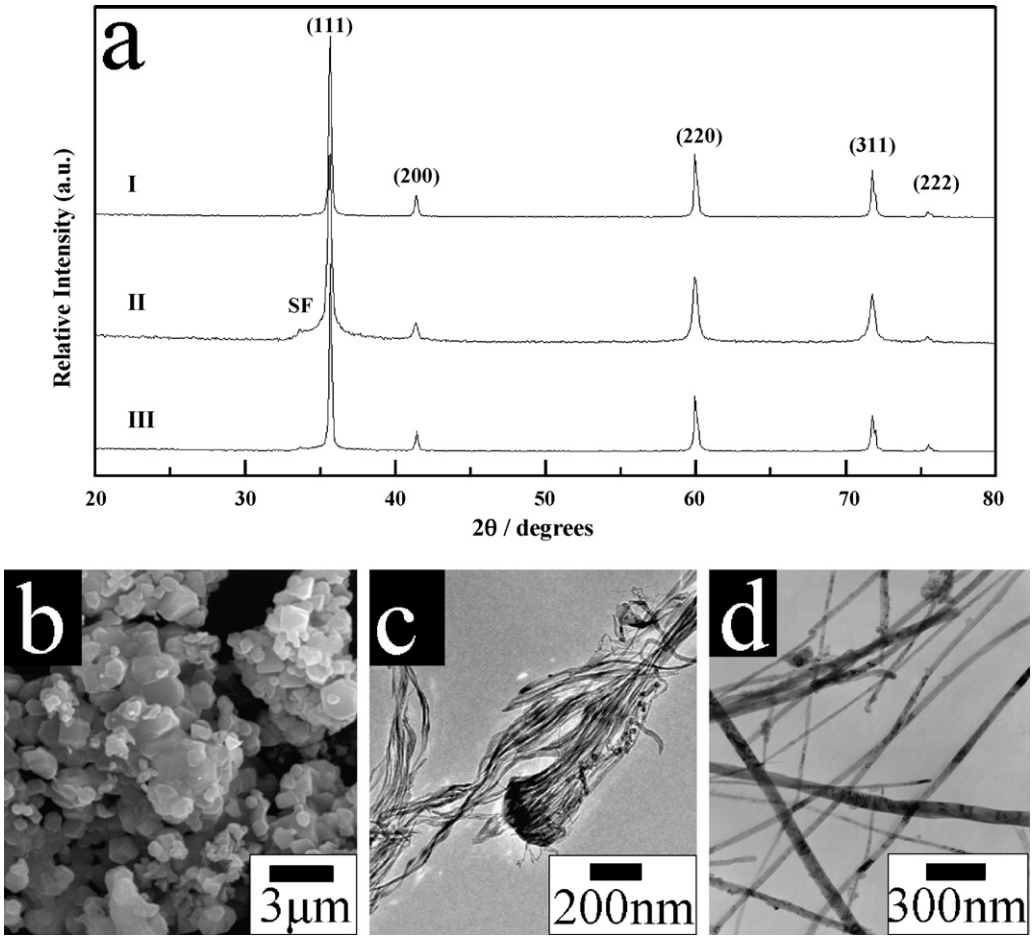

Fig. 9. (a) XRD patterns of the samples synthesized by three different systems: I: CHI_3/Si/K/at 140 °C for 20 h; II: CBr_4/Si/Na at 300 °C for 20 h; III: $CHCl_3$/Si/Na at 350 °C for 48 h. (b) The typical SEM image of Sample obtained from system I. (c) TEM image of Sample obtained from system II. (d) TEM image of Sample obtained from system III.

tern of the obtained product in Fig. 9a (I) can be indexed as 3C-SiC. However, the obtained product is mainly composed of irregular polyhedron-like structures (Fig. 9b). If metallic Mg was used instead of Na as the reactant, no SiC could be obtained even the temperature was elevated up to 600 °C. SiC nanowires also could be prepared by using $CHCl_3$ and CBr_4 instead of CHI_3 in our experiment (see Fig. 9c and d), Fig. 9a (II, III) shows the XRD patterns of the two products, which can be assigned to 3C-SiC. Whereas, both the ratio of the nanowires (70%) in the two products are lower than Sample 1 (80%).

4. Conclusions

In this paper, cubic SiC nanowires and micro-scaled polyhedra have been synthesized by using Si powder, CHI_3, and metallic Na at 230 °C and 500 °C, respectively. At room temperature, strong ultraviolet emissions at 360 nm and 354 nm are found in the as-obtained SiC nanowires and micro-scaled polyhedra. TGA curves reveal that the thermal stability of the micro-scaled polyhedra is better than nanowires. Owing to their intensive ultraviolet emission and superior thermal stability, the as-synthesized samples may have potential applications in ultraviolet light-emitting diodes and extreme environmental conditions especially at high temperature.

Acknowledgements

This work was supported by National Natural Science Found of China (Nos.: 20871075, 20971079), the 973 Project of China (No. 2005CB623601), the Taishan Scholar Project of Shandong

Province, and Independent Innovation Foundation of Shandong University.

References

[1] A.O. Konstantinov, Q. Wahab, N. Nordell, U. Lindefeltal, Appl. Phys. Lett. 71 (1997) 90.
[2] V.D. Krstic, J. Am. Ceram. Soc. 75 (1992) 170.
[3] Z.L. Wang, Z.R. Dai, R.P. Gao, Z.G. Bai, Appl. Phys. Lett. 77 (2000) 3349.
[4] G.C. Xi, R.J. Yu, R. Zhang, M. Zhang, D.K. Ma, Y.T. Qian, J. Phys. Chem. B 109 (2005) 13200.
[5] T. Ito, K. Sano, T. Akiyama, K. Nakamura, Thin Solid Films 508 (2006) 243.
[6] M.V. William, D. Michael, J. Cryst. Growth 260 (2004) 201.
[7] T. Furusho, M. Sasaki, S. Ohshima, S. Nishino, J. Cryst. Growth 249 (2003) 216.
[8] W. Yang, H. Arki, C. Tang, S. Thaveethavorn, A. Kohyama, H. Suzuki, T. Noda, Adv. Mater. 17 (2005) 1519.
[9] P. Li, L.Q. Xu, Y.T. Qian, Cryst. Growth Des. 8 (2008) 2431.
[10] H.J. Dai, E.W. Wong, Y.Z. Lu, S.S. Fan, C.M. Lieber, Nature 375 (1995) 769.
[11] J.Q. Hu, Q.Y. Lu, K.B. Tang, Y.T. Qian, G.E. Zhou, X.M. Liu, J.X. Wu, Chem. Mater. 11 (1999) 2369–2371.
[12] Y.B. Li, P.S. Dorozhkin, Y. Bando, D. Golberg, Adv. Mater. 17 (2005) 545.
[13] C.C. Tang, Y. Bando, Appl. Phys. Lett. 83 (2003) 659.
[14] J.Q. Hu, Q.Y. Lu, K.B. Tang, B. Deng, R.R. Jiang, Y.T. Qian, W.C. Yu, G.E. Zhou, X.M. Liu, J.X. Wu, J. Phys. Chem. B 104 (2000) 5251.
[15] E. BorowiakPalen, M.H. Ruemmeli, T. Gemming, M. Knupfer, K. Biedermann, A. Leonhardt, T. Pichler, R.J. Kalenczuk, J. Appl. Phys. 97 (2005) 056102.
[16] G.Z. Shen, D. Chen, K.B. Tang, Chem. Phys. Lett. 375 (2003) 177.
[17] G. Gundiah, G.V. Madhav, A. Govindaraj, M.M. Seikh, C.N.R. Rao, J. Mater. Chem. 12 (2002) 1606.
[18] J.Q. Hu, Y. Bando, J.H. Zhan, D. Golberg, Appl. Phys. Lett. 85 (2004) 2932.
[19] G.C. Xi, Y.Y. Peng, S.M. Wan, T.W. Li, W.C. Yu, Y.T. Qian, J. Phys. Chem. B 108 (2004) 20102.
[20] C.H. Liang, G.W. Meng, L.D. Zhang, Y.C. Wu, Z. Cui, Chem. Phys. Lett. 329 (2000) 323.
[21] M. Ohkohchi, Y. Ando, J. Ceram. Soc. Japan 98 (1990) 417.
[22] Y. Ando, M. Ohkohchi, Jpn. J. Appl. Phys. 29 (1990) 2429.
[23] Y.G. Yang, R.B. Wu, J.J. Chen, M.X. Gao, R. Zhai, L.L. Wu, J. Lin, Y. Pan, J. Zhejiang Uni. (Eng. Sci.) 41 (2007) 1042.
[24] D. Chaussende, F. Mercier, A. Boulle, F. Conchon, M. Soueidan, G. Ferro, A. Mantzari, A. Andreadou, E.K. Polychroniadis, C. Balloud, S. Juillaguet, J. Camassel, M. Pons, J. Cryst. Growth 310 (2008) 976–981.
[25] H.P. Martin, R. Ecke, E. Muller, J. Eur. Ceram. Soc. 18 (1998) 1737–1742.
[26] J. Narayan, R. Raghunathan, R. Chowdhury, K. Jagannadham, J. Appl. Phys. 75 (1994) 7252–7257.
[27] I.S. Seog, C.H. Kim, J. Mater. Sci. 28 (1993) 3277–3282.
[28] C. Vix-Guterl, P. Ehrburger, Carbon 35 (1997) 1587–1592.
[29] G.W. Meng, Z. Cui, L.D. Zhang, F. Phillipp, J. Cryst. Growth 209 (2000) 801.
[30] Z.C. Ju, Z. Xing, C.L. Guo, L.S. Yang, L.Q. Xu, Y.T. Qian, Eur. J. Inorg. Chem. 24 (2008) 3883.
[31] T. Li, L.Q. Xu, L.C. Wang, L.S. Yang, Y.T. Qian, J. Alloys Compd. 484 (2009) 341.
[32] K. Koumoto, S. Takeda, C. Pai, T. Sata, H. Yanagida, J. Am. Ceram. Soc. 72 (1989) 1985.
[33] L.S. Liao, X.M. Bao, Z.F. Yang, N.B. Min, Appl. Phys. Lett. 66 (1995) 2382.
[34] D.L. Ou, A.B. Seddon, J. Non-Cryst. Solids 210 (1997) 187.
[35] X.H. Wang, L. Wang, L.Q. Wong, Q. Wang, H. Wang, G.A. Tai, Funct. Mater. 35 (2004) 2995.
[36] D. Olego, M. Cardona, Phys. Rev. B 25 (1982) 3889.
[37] Z.C. Feng, A.J. Mascarenhas, W.J. Choyke, J.A. Powell, J. Appl. Phys. 64 (1988) 3176.
[38] Z.X. Yang, Y.D. Xia, M. Robert, Chem. Mater. 16 (2004) 3877.
[39] R. Moene, M. Makkee, J.A. Moulijn, Appl. Catal. A 167 (1998) 321.
[40] Y. Yao, S.T. Lee, F.H. Li, Chem. Phys. Lett. 381 (2003) 628.
[41] H.W. Shim, K.C. Kim, Y.H. Seo, Appl. Phys. Lett. 70 (1997) 1757.
[42] J.J. Chen, R.B. Wu, G.Y. Yang, Y. Pan, J. Lin, L.L. Wu, R. Zhai, J. Alloys Compd. 456 (2008) 320.
[43] N. Keller, C. Pham-Huu, S. Roy, M.J. Ledoux, J. Mater. Sci. 34 (1999) 3189.
[44] J. Gravesena, M. Willatzenb, Physica B 371 (2006) 112.
[45] X.C. Zhang, S.X. Qu, J. Shannxi Nor. Uni (Nat. Sci. Ed.) 36 (2008) 33.
[46] R.S. Wagner, W.C. Ellis, Appl. Phys. Lett. 4 (1964) 89.
[47] Y. Cui, L.J. Lauhon, M.S. Gudiksen, Appl. Phys. Lett. 78 (2001) 2214.
[48] Z.G. Ju, Y.M. Lu, J.Y. Zhang, X.J. Wu, K.W. Liu, C.X. Shan, B.S. Li, D.X. Zhao, Z.Z. Zhang, B.H. Li, B. Yao, D.Z. Shen, Cryst. Growth Des. 8 (2008) 2733.
[49] Y.H. Tong, Y.C. Liu, C.L. Shao, R.X. Wu, Appl. Phys. Lett. 88 (2006) 123111.
[50] W.J. Li, E.W. Shi, Z.Z. Chen, Z.W. Yin, Sci. China Ser. B 44 (2001) 123.